

Discovery of a new supernova remnant G150.3+4.5

X. Y. Gao and J. L. Han

National Astronomical Observatories, CAS, Jia-20 Datun Road, Chaoyang District, Beijing 100012, PR China

Received 06 May 2014; accepted 04 June 2014

ABSTRACT

Context. Large-scale radio continuum surveys have good potential for discovering new Galactic supernova remnants (SNRs). Surveys of the Galactic plane are often limited in the Galactic latitude of $|b| \sim 5^\circ$. SNRs at high latitudes, such as the Cygnus Loop or CTA 1, cannot be detected by surveys in such limited latitudes.

Aims. Using the available Urumqi $\lambda 6$ cm Galactic plane survey data, together with the maps from the extended ongoing $\lambda 6$ cm medium latitude survey, we wish to discover new SNRs in a large sky area.

Methods. We searched for shell-like structures and calculated radio spectra using the Urumqi $\lambda 6$ cm, Effelsberg $\lambda 11$ cm, and $\lambda 21$ cm survey data. Radio polarized emission and evidence in other wavelengths are also examined for the characteristics of SNRs.

Results. We discover an enclosed oval-shaped object G150.3+4.5 in the $\lambda 6$ cm survey map. It is about 2.5° wide and 3° high. Parts of the shell structures can be identified well in the $\lambda 11$ cm, $\lambda 21$ cm, and $\lambda 73.5$ cm observations. The Effelsberg $\lambda 21$ cm total intensity image resembles most of the structures of G150.3+4.5 seen at $\lambda 6$ cm, but the loop is not closed in the northwest. High resolution images at $\lambda 21$ cm and $\lambda 73.5$ cm from the Canadian Galactic Plane Survey confirm the extended emission from the eastern and western shells of G150.3+4.5. We calculated the radio continuum spectral indices of the eastern and western shells, which are $\beta \sim -2.4$ and $\beta \sim -2.7$ between $\lambda 6$ cm and $\lambda 21$ cm, respectively. The shell-like structures and their non-thermal nature strongly suggest that G150.3+4.5 is a shell-type SNR. For other objects in the field of view, G151.4+3.0 and G151.2+2.6, we confirm that the shell-like structure G151.4+3.0 very likely has a SNR origin, while the circular-shaped G151.2+2.6 is an H II region with a flat radio spectrum, associated with optical filamentary structure, H α , and infrared emission.

Key words. Radio continuum: ISM – ISM: supernova remnants – ISM: individual objects: G150.3+4.5

1. Introduction

There is a large discrepancy between the theoretically predicted numbers of the Galactic supernova remnants (SNRs) (e.g., Berkhuysen 1984; Li et al. 1991; Tammann et al. 1994) and the observational detections (Green 2009; Ferrand & Safi-Harb 2012), which is often attributed to the limitations of the current observations on the angular resolutions to detect distant small SNRs, the sensitivities to reveal faint SNRs, and the insufficient sky coverage for the completeness of detections. In addition, strong confusion from the diffuse Galactic emission makes discoveries of SNRs in the inner Galaxy even more difficult.

Previously, the big steps in the discovery of the Galactic SNRs relied on the radio surveys carried out by powerful telescopes, e.g., Shaver & Goss (1970) and Clark et al. (1975) on the 408 MHz and 5 GHz surveys by the Parkes and Molonglo telescopes. Reich et al. (1988) found many SNRs using the $\lambda 21$ cm and $\lambda 11$ cm surveys made by the Effelsberg 100-m telescope. With the Molonglo telescope again, Whiteoak & Green (1996) identified SNRs with the 843 MHz survey data. The most recent significant increase in the number of the Galactic SNRs was made by Brogan et al. (2006), using the high angular resolution of the VLA to detect 35 new SNRs in the inner Galaxy. There are also some individual discoveries, although not many. The Sino-German $\lambda 6$ cm polarisation survey of the Galactic plane¹ (Sun et al. 2007; Gao et al. 2010; Sun et al. 2011a; Xiao et al. 2011) conducted by the Urumqi 25-m radio telescope provides a good hunting ground for dis-

covering new Galactic SNRs. Gao et al. (2011) identified two new faint SNRs G25.1–2.3 and G178.2–4.2. Supplemented by the Urumqi $\lambda 6$ cm data, Foster et al. (2013) identified another two new SNRs G152.4–2.1 and G190.9–2.2 from the Canadian Galactic Plane Survey (CGPS) data. With the Giant Meterwave Radio Telescope, Roy & Pal (2013) have recently discovered a young SNR G354.4+0.0 in the central region of the Galaxy. The CGPS has also contributed several other detections, e.g. G85.4+0.7 and G85.9–0.6 by Kothes et al. (2001), G107.5–1.5 by Kothes (2003), G96.0+2.0 and G113.0+0.2 by Kothes et al. (2005), G108.2–0.6 by Tian et al. (2007), and G141.2+5.0 by Kothes et al. (2014). However, most of the radio continuum surveys of the Galactic plane are limited in a latitude range, e.g. $|b| \leq 5^\circ$. This is not sufficient to discover and study the SNRs off the plane, such as the Cygnus Loop (G74.0–8.5) (e.g., Harris & Roberts 1960; Sun et al. 2006) and the CTA 1 (G119.5+10.2) (e.g., Walsh & Brown 1955; Sun et al. 2011b).

Following the Urumqi $\lambda 6$ cm plane survey, a survey extending the latitude range from $b = 5^\circ$ to $b = 20^\circ$ has been carried out since 2012 (Gao et al. in prep.). It currently collects the data of $\lambda 6$ cm total intensity and linear polarization from the longitude range from $\ell = 90^\circ$ to 160° . Here we report the discovery of a new SNR G150.3+4.5 by combing the new data with the $\lambda 6$ cm plane survey data. We introduce the data in Sect. 2. The radio continuum emission, the spectrum, and the evidence collected in other bands are discussed in Sect. 3. We summarize our work in Sect. 4.

Send offprint requests to: bearwards@gmail.com

¹ <http://zmtt.bao.ac.cn/6cm/>

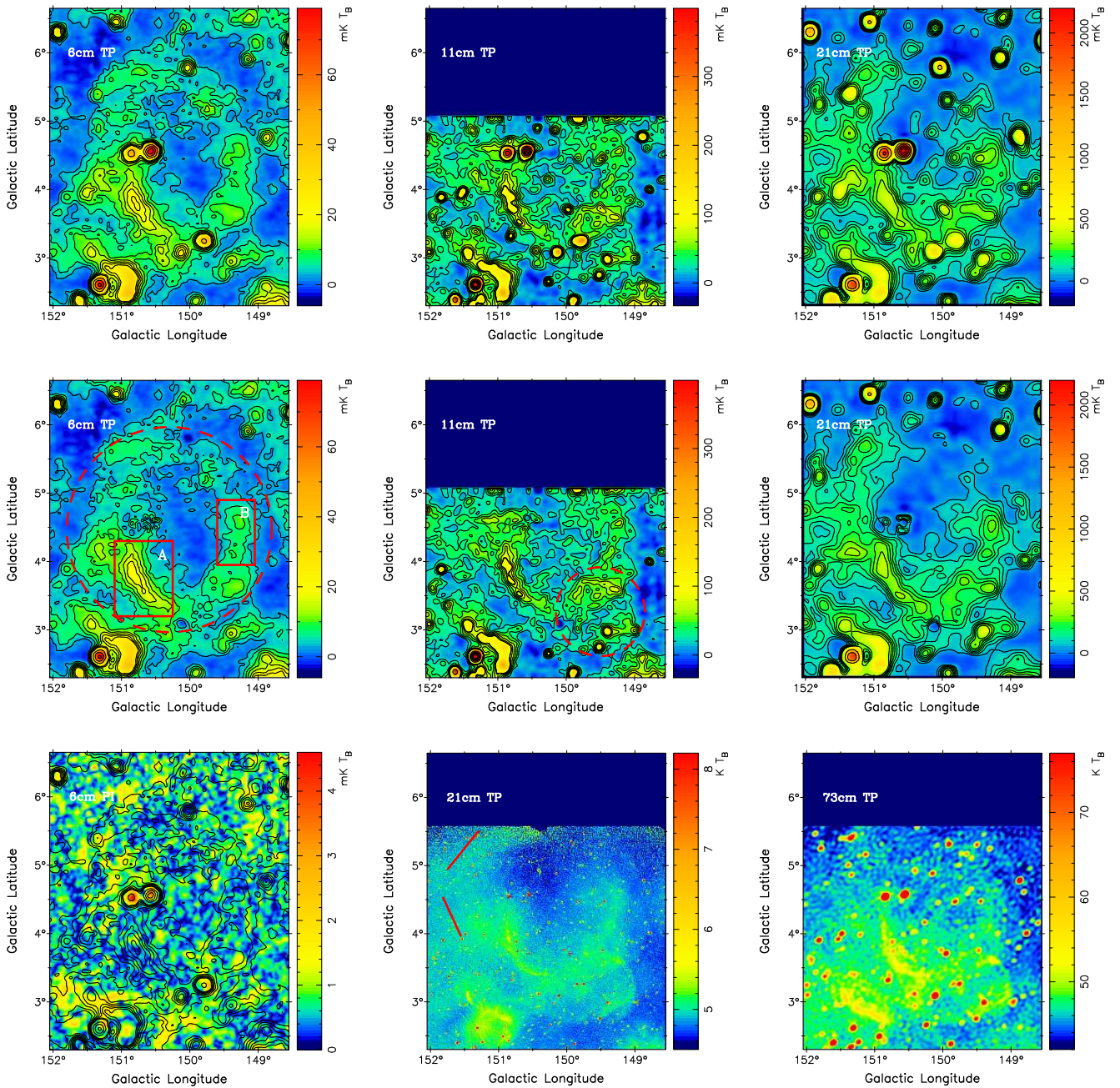


Fig. 1. Radio continuum images of the new SNR G150.3+4.5. *Top panels:* total intensity of G150.3+4.5 obtained from Urumqi $\lambda 6$ cm (*left*), Effelsberg $\lambda 11$ cm (*central*), and Effelsberg $\lambda 21$ cm (*right*) observations. The contours run at $3.0 + (n-1) \times 3.0$ mK ($n=1, 2, \dots, 6$) and $21.0 + (n-7) \times 21.0$ mK ($n=7, 8, \dots$) for the $\lambda 6$ cm image, at $20.0 + (n-1) \times 13.4$ mK ($n=1, 2, \dots, 6$) and $85.0 + (n-7) \times 212.0$ mK ($n=7, 8, \dots$) for the $\lambda 11$ cm image, at $60.0 + (n-1) \times 40.0$ mK ($n=1, 2, \dots, 6$) and $320.0 + (n-7) \times 600.0$ mK ($n=7, 8, \dots$) for the $\lambda 21$ cm image. *Middle panels:* the same images as *upper panels*, but point-like sources are removed within the central 3° field as indicated by the circle in the left panel. *Bottom panels:* images for the $\lambda 6$ cm polarization intensity (*left*), the CGPS $\lambda 21$ cm total intensity (*central*) and $\lambda 73.5$ cm total intensity (*right*). The contours on the $\lambda 6$ cm polarisation image is the same as for the $\lambda 6$ cm total intensity image shown in the *upper panels*. The angular resolutions for observations of the Urumqi $\lambda 6$ cm, Effelsberg $\lambda 21$ cm, CGPS $\lambda 21$ cm, and $\lambda 73.5$ cm images are $9''.5, 9''.4, 60'' \times 49''$, and $3''.5 \times 2''.8$, respectively. The Effelsberg $\lambda 11$ cm image was convolved to the resolution of $6'$ to increase the signal-to-noise ratio. The rectangles A and B as indicated in the *middle left panel* are the areas for TT plots in Fig. 2. The dashed circle in the *middle central panel* indicates the newly discovered SNR G149.5+3.2 by Gerbrandt et al. (2014), which overlaps with the lower part of the western shell of G150.3+4.5. The two straight lines shown in the CGPS $\lambda 21$ cm total intensity image indicate the emission, which does not seem to be connected to the eastern shell of G150.3+4.5.

2. Data

2.1. Urumqi $\lambda 6$ cm data

The $\lambda 6$ cm total intensity I and the linear polarization U and Q data used in this paper come from a portion of the Sino-German

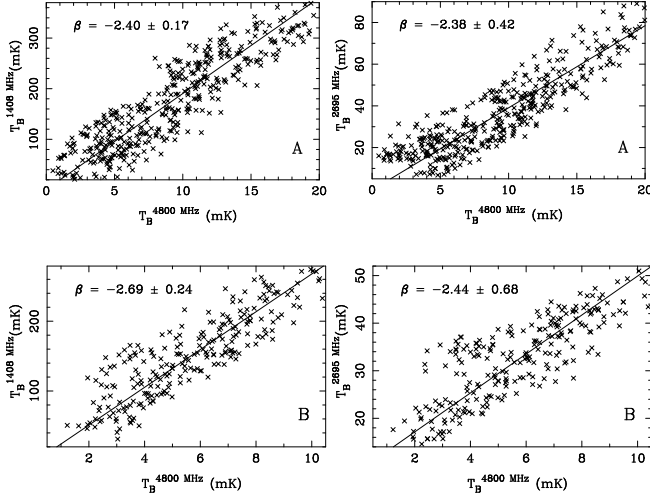


Fig. 2. TT plots between $\lambda 6$ cm and $\lambda 21$ cm and between the $\lambda 6$ cm and $\lambda 11$ cm for the eastern shell, i.e., region A (*upper panels*), and western shell, i.e., region B (*lower panels*) of G150.3+4.5, as indicated by the rectangles in Fig. 1.

$\lambda 6$ cm polarization survey of the Galactic plane (Gao et al. 2010) and the extended survey with the latitude range from $b = 5^\circ$ to $b = 20^\circ$. Observations of both surveys were made with the same $\lambda 6$ cm system mounted on the Urumqi 25-m radio telescope, Xinjiang Astronomical Observatories, Chinese Academy of Sciences. The observation strategy, data reduction, and calibration follow the same procedures, which have been described in detail in Sun et al. (2007) and Gao et al. (2010). The angular resolution of the $\lambda 6$ cm map is $9'.5$. The sensitivity is about 1.0 mK T_b for total intensity and about 0.3 mK T_b for polarization.

2.2. Effelsberg $\lambda 11$ cm data

The $\lambda 11$ cm total intensity map is a part of the radio continuum survey of the Galactic plane made by the Effelsberg 100-m radio telescope (Fürst et al. 1990). We extracted the data from the survey sampler of the Max-Planck-Institut für Radioastronomie². The map has an angular resolution of $4'.3$. We measured 6.7 mK T_b as the r.m.s. (1σ) for the $\lambda 11$ cm total intensity data.

2.3. Effelsberg $\lambda 21$ cm data

The $\lambda 21$ cm radio continuum data was observed by the Effelsberg telescope for two parts: the data above the latitude of $b = 4^\circ$ come from the Effelsberg Medium Latitude Survey (EMLS) (Uyaniker et al. 1998; Reich et al. 2004), while the data below $b = 4^\circ$ come from the Effelsberg $\lambda 21$ cm radio continuum plane survey (Reich et al. 1997). The angular resolution is about $9'.4$, comparable to that of the $\lambda 6$ cm data. The r.m.s. of the map is about 20.0 mK T_b .

2.4. Canadian $\lambda 21$ cm & $\lambda 73.5$ cm data

Both of the Canadian $\lambda 21$ cm (1420 MHz) and $\lambda 73.5$ cm (408 MHz) data are from the Canadian Galactic Plane Survey (CGPS) conducted by the synthesis telescopes of the Dominion Radio Astronomical Observatory (DRAO) (Taylor et al. 2003; Landecker et al. 2010). The data were extracted from the the

Canadian astronomy data center³. The $\lambda 21$ cm (1420 MHz) data has an angular resolution of $60'' \times 49''$ in the area of $\ell = 150.3, b = 4.5$, while the $\lambda 73.5$ cm (408 MHz) data has a beam of $3'.5 \times 2'.8$. In this paper, we use the CGPS maps for qualitative study and for showing fine structures on small scales.

3. Results

We present the Urumqi $\lambda 6$ cm, the Effelsberg $\lambda 11$ cm, and the Effelsberg $\lambda 21$ cm total intensity images of a $3'.5 \times 4'.35$ region around the target in the top panels of Fig. 1. The loop structure seen from the $\lambda 6$ cm image is named G150.3+4.5, according to its geometric center. To study the faint and extended emission of this object, prominent point-like sources ($S_{1.4\text{GHz}} > 20$ mJy) within the central field of 3° are subtracted based on the NVSS source catalog (Condon et al. 1998). For point-like sources that have determined radio flux density spectral indices ($S_\nu = \nu^\alpha$) (Vollmer et al. 2005), we simply extrapolate the flux densities from 1.4 GHz to the other two frequencies. For sources with unknown spectral indices, a spectral index of $\alpha = -0.9$ is used for extrapolation. We show the total intensity images in the middle panels of Fig. 1 for the $\lambda 6$ cm, $\lambda 11$ cm and the Effelsberg $\lambda 21$ cm bands after the point-like sources are removed. The $\lambda 6$ cm polarization image and the high resolution total intensity images of the DRAO $\lambda 21$ cm and $\lambda 73.5$ cm are shown in the bottom panels of Fig. 1. The currently available radio continuum observations of the Effelsberg $\lambda 11$ cm data ends up at $b = 5^\circ$, while the DRAO $\lambda 21$ cm and $\lambda 73.5$ cm data extend to about $b = 5'.5$. The angular resolutions of the $\lambda 6$ cm, the Effelsberg $\lambda 21$ cm, the DRAO $\lambda 21$ cm, and the DRAO $\lambda 73.5$ cm images are $9'.5$, $9'.4$, $60'' \times 49''$ and $3'.5 \times 2'.8$, respectively. To increase the signal-to-noise ratio, the Effelsberg $\lambda 11$ cm total intensity image was convolved to an angular resolution of $6'$.

3.1. Total intensity and the spectral index

The big loop G150.3+4.5 is clearly seen in the Urumqi $\lambda 6$ cm and the Effelsberg $\lambda 21$ cm images, extending to a higher latitude of more than $b = 6^\circ$. It shows an enclosed oval shape at $\lambda 6$ cm, which is about $2'.5$ wide and $3'$ high. Three major shells of G150.3+4.5 can be identified in the $\lambda 6$ cm image. The most prominent one is found in the east, curving to the center of the lower south, while a fainter shell can be identified in the west, also extending to the lower south. A much fainter and fragmented shell is found in the upper north. From the $\lambda 6$ cm map after subtracting the point-like sources, we see the emission in that region is just around 3σ (~ 3.0 mK T_b) detection above the background.

Most of the structures seen at $\lambda 6$ cm also appear in the Effelsberg $\lambda 21$ cm total intensity map, but the loop is not closed, with a gap in the northwest. This part is detected at $\lambda 6$ cm to be about 3.0 mK T_b , but below $3\sigma_{21\text{cm}} = 60$ mK T_b at $\lambda 21$ cm (see Fig. 1), which indicates that the brightness spectral index of this gap region is shallower than $\beta = -2.46$ ($S_\nu = \nu^\alpha$, $\beta = \alpha - 2$).

The $\lambda 11$ cm data cover only the lower part of G150.3+4.5, but reveals more detailed structures with a $6'$ angular resolution. The new SNR G149.5+3.2, as indicated in Fig. 1 has just been discovered by Gerbrandt et al. (2014). It overlaps with the lower part of the western shell of G150.3+4.5.

The DRAO $\lambda 21$ cm image has the sharpest resolution. The eastern shell of G150.3+4.5 can be traced clearly. The overlap of the lower part of the western shell with the new SNR G149.5+3.2

² <http://www3.mpifr-bonn.mpg.de/survey.html>

³ <http://www1.cadc-ccda.hia-ihp.nrc-cnrc.gc.ca/cgps/query.html>

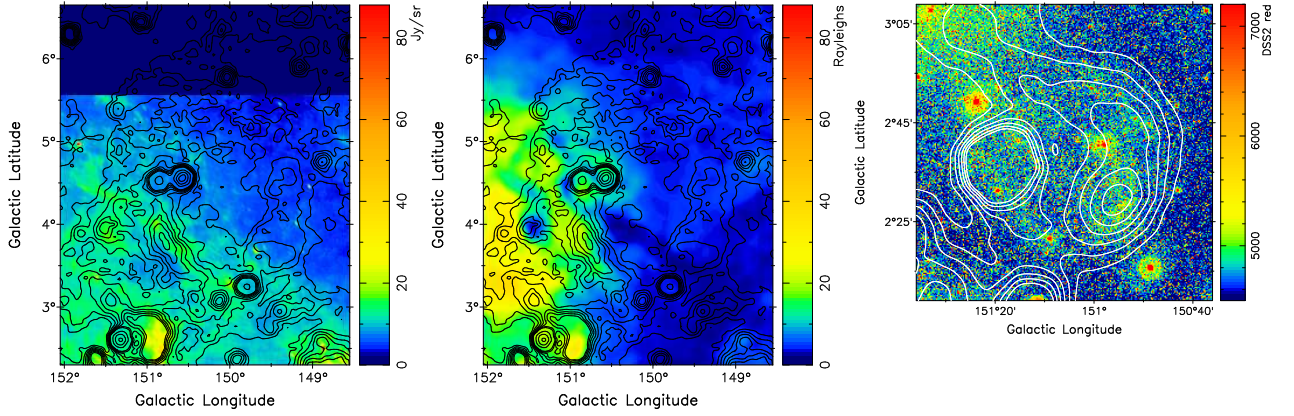


Fig. 3. 60 μ m infrared (*left panel*) and H α emission (*middle panel*) in the area of G150.3+4.5. The contours are the same for the $\lambda 6$ cm image shown in the *upper panel* of Fig. 1. *Right panel*: optical emission from the DSS2 red image in the field of G151.2+2.6. $\lambda 6$ cm total intensity contours run at 6.0 mK T_b in steps of 6.0 mK T_b .

(Gerbrandt et al. 2014) is clearly seen. The upper part of the western shell, free of the contamination of G149.5+3.2, can be identified above $b = 4^\circ$. The fragmented northern shell of G150.3+4.5 seen at $\lambda 6$ cm cannot be identified. From the $\sim 1'$ resolution map, there is no continuous emission of the prominent eastern shell pointing to the north. Faint extended emission goes wider from $\ell = 151^\circ 3', b = 4^\circ 1'$ to $\ell = 151^\circ 6', b = 4^\circ 5'$ and then turns to $\ell = 150^\circ 9', b = 5^\circ 4'$ (as indicated in Fig. 1). As for the Effelsberg $\lambda 21$ cm map, the DRAO $\lambda 21$ cm observations do not detect the emission in the northwest of the loop, either.

The DRAO $\lambda 73.5$ cm image revealed the prominent eastern shell. The western shell of G150.3+4.5 appears to be fainter. The new SNR G149.5+3.2 can also be identified in the lower right of G150.3+4.5.

Gerbrandt et al. (2014) demonstrate the non-thermal synchrotron emission nature of the eastern shell of G150.3+4.5 and propose that it is a new SNR. We tested it with the TT-plot method (Turtle et al. 1962), using the Urumqi $\lambda 6$ cm, the Effelsberg $\lambda 11$ cm, and the Effelsberg $\lambda 21$ cm data. We got the brightness temperature spectral index of $\beta = -2.40 \pm 0.17$ between the $\lambda 6$ cm and $\lambda 21$ cm data, and $\beta = -2.38 \pm 0.42$ between the $\lambda 6$ cm and $\lambda 11$ cm data, which are consistent with the result of Gerbrandt et al. (2014). The western shell of G150.3+4.5 is not mentioned in Gerbrandt et al. (2014). It can be identified from all total intensity images at various wavelengths as we showed. This shell and the eastern one both curve to the southern lower section, suggesting that they are from the same entity. For the emission that is free of the contamination by the new SNR G149.5+3.2 (see the rectangle area b as indicated in Fig. 1), we tested the spectrum of the upper part of the western shell of G150.3+4.5. TT plots give a spectral index of $\beta = -2.69 \pm 0.24$ between the Urumqi $\lambda 6$ cm and the Effelsberg $\lambda 21$ cm data, and $\beta = -2.44 \pm 0.68$ between the Urumqi $\lambda 6$ cm and Effelsberg $\lambda 11$ cm data, indicating a non-thermal nature.

3.2. Other noticeable structures

Three noticeable structures other than the new SNR G150.3+4.5 are well resolved in the $\sim 1'$ resolution CGPS $\lambda 21$ cm data. They are all located in the lower left hand corner of the maps in Fig. 1 and collected by Kerton et al. (2007) in the CGPS extended source catalog. G151.2+2.6 (CGPSE 169) has a circular shape with a size of about $40'$, while G150.9+2.7 (CGPSE 168) and G151.4+3.0 (CGPSE 172) both have an arc shape with

a length of about $20'$. G151.2+2.6, however, is not detected at 408 MHz. Thus its nature is still unclear. Based on the steep non-thermal spectral indices found between 408 MHz and 1420 MHz CGPS data ($\alpha = -1.3 \pm 0.3$ for G150.9+2.7, $\alpha = -0.4 \pm 0.2$ for G151.4+3.0), Kerton et al. (2007) propose that the two arcs G150.9+2.7 and G151.4+3.0 form a new Galactic SNR G151.20+2.85.

In the Urumqi and Effelsberg maps with a $\sim 10'$ resolution, the circular G151.2+2.6 can be recognized in all three frequency maps. G150.9+2.7 is mixed with the upper part of G151.2+2.6 and cannot be distinguished. Instead of being an arc, G151.4+3.0 is seen to be an elongated point-like source.

To know their properties, we determined the spectra first. We subtracted the point-like sources from the Urumqi $\lambda 6$ cm, the Effelsberg $\lambda 11$ cm and the Effelsberg $\lambda 21$ cm data based on the NVSS catalog. For the circular G151.2+2.6, to avoid the contamination from G150.9+2.7, the TT plot is only made for the region below $b = 2^\circ 6'$. We obtained the brightness temperature spectral index of $\beta = -2.03 \pm 0.32$ between $\lambda 6$ cm and $\lambda 11$ cm, and $\beta = -2.18 \pm 0.08$ between $\lambda 6$ cm and $\lambda 21$ cm. The flat radio continuum spectrum implies that G151.2+2.6 may have a thermal origin.

For G150.9+2.7, we cannot see it owing to the overlap with G151.2+2.6. For the source G151.4+3.0, a non-thermal spectral index is found to be $\beta = -2.62 \pm 0.15$ between the $\lambda 6$ cm and $\lambda 21$ cm data, supporting the idea of Kerton et al. (2007) that G151.4+3.0 is a (part of) SNR.

3.3. Hints in other bands

We search for coincidence of the objects we discussed in infrared, H α , and DSS2 red maps (McLean et al. 2000). From the ancillary 60 μ m infrared map downloaded from the CGPS website, except for the western part of G151.2+2.6, we do not see any strong correlations between the infrared and the radio continuum emission toward any extended objects in Fig. 1 (see Fig. 3, *left panel*). Kerton et al. (2007) suggest that there is related infrared emission in the eastern shell of G150.3+4.5. Together with the flat spectral index they derived, the eastern shell was said to be an HII region. We agree with Gerbrandt et al. (2014) that the strong overall infrared emission does not appear to be correlated with the eastern shell of the new SNR G150.3+4.5.

We extracted the $H\alpha$ image from the Wisconsin $H\alpha$ mapper northern sky survey (Haffner et al. 2003). Again we do not see any firm correlation with any structures except for some parts of G151.2+2.6 (Fig. 3, *middle panel*). Strong $H\alpha$ emission is seen in the eastern part of the image, and it overlaps with the eastern shell of the new SNR G150.3+4.5. This could possibly explain the non-detection of the polarized emission at $\lambda 6$ cm as a result of depolarization, if the magneto-ionized medium appears as the foreground.

From the DSS2 red image, Gerbrandt et al. (2014) show that an optical filamentary structure is coincident with the lower part of the eastern shell of G150.3+4.5. For the other parts of G150.3+4.5, we do not see this coincidence. A ring-shaped optical counterpart is found for G151.2+2.6 (see Fig. 3, *right panel*). This, together with the flat radio continuum spectrum, the $H\alpha$, and infrared emission, strongly suggest that it is an H II region.

4. Summary

By combining the Urumqi $\lambda 6$ cm Galactic plane survey and the new medium latitude survey, we discovered an enclosed oval-shaped object G150.3+4.5. It contains three shells in the east, west, and north, respectively. Effelsberg $\lambda 11$ cm and $\lambda 21$ cm radio continuum data are used for the spectral index analysis, and the high angular resolution CGPS $\lambda 21$ cm and $\lambda 73.5$ cm data are used for its fine structure. The eastern and western shells of G150.3+4.5 can be firmly confirmed, while the faint northern shell seen at $\lambda 6$ cm has not been detected in other radio frequencies.

The TT plots between $\lambda 6$ cm, $\lambda 11$ cm, and $\lambda 21$ cm are employed for analyzing the spectra of the eastern and western shells of the newly discovered loop of G150.3+4.5. We found non-thermal radio spectra for the shells on both sides. The spectral index for the eastern shell is about $\beta \sim -2.4$, and about $\beta \sim -2.7$ for the western shell. From the properties of this half loop and the optical filamentary structure that is related to the eastern radio shell (Gerbrandt et al. 2014), G150.3+4.5 should be a SNR, though the polarized emission from G150.3+4.5 is not detected, which might be due to the sensitivity limit or depolarization effect in the eastern shell.

For the other prominent structures in the observed area, we confirm that the arc structure G151.4+3.0 has a non-thermal spectrum, based on the Urumqi $\lambda 6$ cm and the Effelsberg $\lambda 21$ cm data. This agrees with the result of Kerton et al. (2007) that it has a SNR origin. But from the morphology, it is still not clear G150.9+2.7, and G151.4+3.0 form one SNR or two separated SNRs. We found a flat radio continuum spectrum for the circular G151.2+2.6 and the related $H\alpha$ and infrared emission in its western part, and also the related optical emission in the DSS2 red image, which all suggest that G151.2+2.6 is an H II region.

Acknowledgements. We thank the referee for helpful comments that improved our paper. The authors are supported by the National Natural Science Foundation of China (11303035) and by the Strategic Priority Research Program “The Emergence of Cosmological Structures” of the Chinese Academy of Sciences, Grant No. XDB09010200. X.Y.G is also supported by the Young Researcher Grant of National Astronomical Observatories, Chinese Academy of Sciences. We acknowledge Mr Otmar Lochner for construction of the excellent $\lambda 6$ cm receiver and Mr Maozheng Chen and Jun Ma for their skillful maintenance.

References

Berkhuijsen, E. M. 1984, A&A, 140, 431
Brogan, C. L., Gelfand, J. D., Gaensler, B. M., Kassim, N. E., & Lazio, T. J. W. 2006, ApJ, 639, L25

Clark, D. H., Caswell, J. L., & Green, A. J. 1975, Australian Journal of Physics Astrophysical Supplement, 1
Condon, J. J., Cotton, W. D., Greisen, E. W., et al. 1998, AJ, 115, 1693
Ferrand, G., & Safi-Harb, S. 2012, Advances in Space Research, 49, 1313
Foster, T. J., Cooper, B., Reich, W., Kothes, R., & West, J. 2013, A&A, 549, A107
Fürst, E., Reich, W., Reich, P., & Reif, K. 1990, A&AS, 85, 691
Gao, X. Y., Reich, W., Han, J. L., et al. 2010, A&A, 515, A64
Gao, X. Y., Sun, X. H., Han, J. L., et al. 2011, A&A, 532, A144
Gerbrandt, S., Foster, T. J., Kothes, R., Geisbuesch, J., & Tung, A. 2014, ArXiv 1405.1987
Green, D. A. 2009, Bull. Astron. Soc. India, 37, 45
Haffner, L. M., Reynolds, R. J., Tufte, S. L., et al. 2003, ApJS, 149, 405
Harris, D. E., & Roberts, J. A. 1960, PASP, 72, 237
Kerton, C. R., Murphy, J., & Patterson, J. 2007, MNRAS, 379, 289
Kothes, R. 2003, A&A, 408, 187
Kothes, R., Landecker, T. L., Foster, T., & Leahy, D. A. 2001, A&A, 376, 641
Kothes, R., Sun, X. H., Reich, W., & Foster, T. J. 2014, ApJ, 784, L26
Kothes, R., Uyaniker, B., & Reid, R. I. 2005, A&A, 444, 871
Landecker, T. L., Reich, W., Reid, R. I., et al. 2010, A&A, 520, A80
Li, Z., Wheeler, J. C., Bash, F. N., & Jefferys, W. H. 1991, ApJ, 378, 93
McLean, B. J., Greene, G. R., Lattanzi, M. G., & Pirenne, B. 2000, in Astronomical Society of the Pacific Conference Series, Vol. 216, Astronomical Data Analysis Software and Systems IX, ed. N. Manset, C. Veillet, & D. Crabtree, 145
Reich, P., Reich, W., & Fürst, E. 1997, A&AS, 126, 413
Reich, W., Fürst, E., Reich, P., & Junkes, N. 1988, in IAU Colloq. 101: Supernova Remnants and the Interstellar Medium, ed. R. S. Roger & T. L. Landecker, 293
Reich, W., Fürst, E., Reich, P., et al. 2004, in The Magnetized Interstellar Medium, ed. B. Uyaniker, W. Reich, & R. Wielebinski, 45
Roy, S., & Pal, S. 2013, ApJ, 774, 150
Shaver, P. A., & Goss, W. M. 1970, Australian Journal of Physics Astrophysical Supplement, 14, 133
Sun, X. H., Han, J. L., Reich, W., et al. 2007, A&A, 463, 993
Sun, X. H., Reich, W., Han, J. L., Reich, P., & Wielebinski, R. 2006, A&A, 447, 937
Sun, X. H., Reich, W., Han, J. L., et al. 2011a, A&A, 527, A74
Sun, X. H., Reich, W., Wang, C., Han, J. L., & Reich, P. 2011b, A&A, 535, A64
Tammann, G. A., Loeffler, W., & Schroeder, A. 1994, ApJS, 92, 487
Taylor, A. R., Gibson, S. J., Peracaula, M., et al. 2003, AJ, 125, 3145
Tian, W. W., Leahy, D. A., & Foster, T. J. 2007, A&A, 465, 907
Turtle, A. J., Pugh, J. F., Kenderdine, S., & Pauliny-Toth, I. I. K. 1962, MNRAS, 124, 297
Uyaniker, B., Fürst, E., Reich, W., Reich, P., & Wielebinski, R. 1998, A&AS, 132, 401
Vollmer, B., Davoust, E., Dubois, P., et al. 2005, A&A, 431, 1177
Walsh, D., & Brown, R. H. 1955, Nature, 175, 808
Whiteoak, J. B. Z., & Green, A. J. 1996, A&AS, 118, 329
Xiao, L., Han, J. L., Reich, W., et al. 2011, A&A, 529, A15